POLITECNICO DI TORINO
Repository ISTITUZIONALE

# Diamond-based sensors for in vitro cellular radiobiology: Simultaneous detection of cell exocytic activity and ionizing radiation

*Original*
Diamond-based sensors for in vitro cellular radiobiology: Simultaneous detection of cell exocytic activity and ionizing radiation / Tomagra, Giulia; Peroni, Giulia; Aprà, Pietro; Bonino, Valentina; Campostrini, Matteo; Carabelli, Valentina; Collà Ruvolo, Cecilia; Lo Giudice, Alessandro; Guidorzi, Laura; Mino, Lorenzo; Olivero, Paolo; Pacher, Luca; Picariello, Fabio; Re, Alessandro; Rigato, Valentino; Truccato, Marco; Varzi, Veronica; Vittone, Ettore; Picollo, Federico. - In: BIOSENSORS & BIOELECTRONICS. - ISSN 0956-5663. - ELETTRONICO. - 220:(2023), pp. 114876-114884. [10.1016/j.bios.2022.114876]
*Availability:*
This version is available at: 11583/2975743 since: 2023-02-07T10:38:54Z

*Publisher:*
Elsevier

*Published*
DOI:10.1016/j.bios.2022.114876

*Terms of use:*

This article is made available under terms and conditions as specified in the corresponding bibliographic description in the repository

*Publisher copyright*

(Article begins on next page)

12 October 2024

Biosensors and Bioelectronics 220 (2023) 114876

Contents lists available at ScienceDirect

Biosensors and Bioelectronics

journal homepage: www.elsevier.com/locate/bios

# Diamond-based sensors for in vitro cellular radiobiology: Simultaneous detection of cell exocytic activity and ionizing radiation

Giulia Tomagra [a,1], Giulia Peroni [b,1], Pietro Aprà [b,c,*], Valentina Bonino [d], Matteo Campostrini [e], Valentina Carabelli [a], Cecilia Collà Ruvolo [b], Alessandro Lo Giudice [b,c], Laura Guidorzi [b,c], Lorenzo Mino [f], Paolo Olivero [b,c], Luca Pacher [b,c], Fabio Picariello [g], Alessandro Re [b,c], Valentino Rigato [e], Marco Truccato [b,c], Veronica Varzi [b,c,h], Ettore Vittone [b,c], Federico Picollo [b,c]

[a] Department of Drug Science and Technology, University of Torino, Corso Raffaello 30, 10125, Torino, Italy
[b] Department of Physics, NIS Inter-departmental Centre, University of Torino, Via Giuria 1, 10125, Torino, Italy
[c] National Institute of Nuclear Physics, Section of Torino, Via Giuria 1, 10125, Torino, Italy
[d] European Synchrotron Radiation Facility – Experiments Division 1 Avenue des Martyrs, F-38000, Grenoble, France
[e] National Institute of Nuclear Physics, National Laboratories of Legnaro, Viale dell'Università, 2 35020, Legnaro, Italy
[f] Department of Chemistry, University of Torino, Via Giuria 7, 10125, Torino, Italy
[g] Department of Electronics and Telecommunications (DET), Polytechnic di Torino, Torino, Italy
[h] Laboratory of Biomedical Technologies, Agenzia Nazionale per le Nuove Tecnologie, l'Energia e lo Sviluppo Economico Sostenibile (ENEA), Via Anguillarese 301, 00123, Roma, Italy

ARTICLE INFO

*Keywords:*
Diamond sensor
Ion beam lithography
Ionizing radiation detection
Dopamine exocytosis
Radiobiology

ABSTRACT

The investigation of secondary effects induced by ionizing radiation represents a new and ever-growing research field in radiobiology. This new paradigm cannot be investigated only using standard instrumentation and methodologies, but rather requires novel technologies to achieve significant progress. In this framework, we developed diamond-based sensors that allow simultaneous real-time measurements with a high spatial resolution of the secretory activity of a network of cells cultured on the device, as well as of the dose at which they are exposed during irradiation experiments. The devices were functionally characterized by testing both the above-mentioned detection schemes, namely: amperometric measurements of neurotransmitter release from excitable cells (such as dopamine or adrenaline) and dosimetric evaluation using different ionizing particles (alpha particle and X-ray photons). Finally, the sensors were employed to investigate the effects induced by X-rays on the exocytotic activity of PC12 neuroendocrine cells by monitoring the modulation of the dopamine release in real-time.

## 1. Introduction

Historically, the predominant paradigm in radiobiology was based on the assumption that the biological effects induced by ionizing radiation are exclusively pertinent to the directly irradiated cell nuclei, and therefore that all the subsequent biological effects (such as the cell death or dysfunction) were strictly correlated with unrepaired or mis-repaired DNA (Steel et al., 1989). In the modern conception, in addition to these direct effects, the relevance of secondary consequences such as bystander and abscopal effects has attracted increasing interest due to several studies that unequivocally highlighted these phenomena (Schaue and Mcbride, 2015). Moreover, numerous research groups are working on the minimization of these phenomena, which are important for cutting-edge fields as for example in the field of FLASH therapy (Durante et al., 2017; Favaudon et al., 2014). Nonetheless, a complete understanding of the mechanisms underlying these effects is still missing and novel systematic investigation approaches are under development (Lacombe et al., 2016; Niklas et al., 2016). In this context, the integration of complementary detection schemes providing a comprehensive description of the interaction between ionizing radiation and living systems is still largely unexplored due to several technological obstacles, despite its paramount importance. Related experiments are generally

* Corresponding author. Department of Physics, NIS Inter-departmental Centre, University of Torino, Via Giuria 1, 10125 Torino, Italy.
*E-mail address:* pietro.apra@unito.it (P. Aprà).
[1] These authors contributed equally to this work.

https://doi.org/10.1016/j.bios.2022.114876
Received 13 September 2022; Received in revised form 20 October 2022; Accepted 31 October 2022
Available online 3 November 2022
0956-5663/© 2022 The Authors. Published by Elsevier B.V. This is an open access article under the CC BY-NC-ND license (http://creativecommons.org/licenses/by-nc-nd/4.0/).

based on assays performed after the irradiation of the biological sample, which inevitably determine the loss of essential information in real-time on the effects occurring during the dose exposure. Our work aims to directly address this substantial topic, thanks to the development of a device of simultaneously measuring the irradiation dose and the biological effect, in real time and with a high temporal and spatial resolution.

To this scope, diamond-based sensors can provide a significant breakthrough due to the outstanding properties of this material. Diamond is a suitable substrate for the development of bioelectronics (Carlisle, 2004; Fan et al., 2020; Krůšek et al., 2019) thanks to its biocompatibility, chemical and electrochemical stability, fouling resistance over multiple acquisition protocols and nonimmunogenic properties (Nistor et al., 2015). Its high biocompatibility allows a significantly better cell adhesion and growth in comparison with standard substrates for electronic, such as silicon and metals (Ariano et al., 2005; Kopecek et al., 2008); the chemical inertness prevents undesired chemical reactions during the sensing processes, and the wide bandgap leads to transparency from near-infrared to far-ultraviolet range, as well as lower electrical noise (Macpherson, 2015). Furthermore, diamond is a suitable material for the fabrication of solid-state particle detectors (Forneris et al., 2013; Oh et al., 2013; Pomorski et al., 2005; Verona et al., 2018), because it offers high radiation hardness due to its extreme bond energy (i.e. 347 kJ $mol^{-1}$), high carrier mobility ($\mu_{electrons} \cong$ (1800–2200) $cm^2$ $V^{-1}$ $s^{-1}$ and $\mu_{holes} \cong$ (2500–3400) $cm^2$ $V^{-1}$ $s^{-1}$ (Gkoumas et al., 2009; Jansen et al., 2013)) guaranteeing fast signal response, lower dielectric constant resulting in better noise performances, high density (i.e. 3.52 g $cm^{-3}$) allowing the fabrication of detectors as thin as 1 μm (Grilj et al., 2013; Skukan et al., 2019), high bandgap (Eg = 5.47 eV) contributing to low thermal noise. Furthermore, in a dosimetric context, diamond offers the advantage of being tissue equivalent, thus providing biologically significant estimations of absorbed dose. Other materials such as silicon, which is widely employed for particle detection, cannot be employed for long-term cell culture, while for example indium tin oxide, although offering optimal properties for biosensing applications, does not allow performing ionizing radiation detection due to the poor charge transport quality of the material.

Different fabrication strategies have been explored for the realization of both diamond-based biosensors and particle detectors, such as conventional lithographic processes for the intrinsic/doped diamond growth (Hébert et al., 2014; Maybeck et al., 2014; McDonald et al., 2017), selective graphitization using high power femtosecond laser irradiation (Bloomer et al., 2020; Lagomarsino et al., 2013) or MeV ion beam lithography (Forneris et al., 2015; Forneris et al., 2013). Laser lithography is widely employed to create graphitic columns through the diamond crystal for the fabrication of particle detectors but, to the best of our knowledge, no papers report on the use of this technology for cellular sensing, most likely due to the poor quality of the electrodes at the surface, which represents a substantial limitation for application in cellular interfacing.

On the other hand, diamond growth represents a widely employed approach for biosensor fabrication since it allows the selective creation of intrinsic (insulating) and doped (conductive) regions.

Meanwhile, in the present work, the MeV ion beam lithography technique was exploited to promote the selective graphitization of diamond and thus create conductive micro-paths embedded within the crystal matrix offering optimal physical-chemical properties for their application as sensing electrodes for cellular release (Carabelli et al., 2017; Picollo et al., 2016b; Tomagra et al., 2019a; 2019c) and as interdigitated particles detectors (Forneris et al., 2014; Olivero et al., 2011), as confirmed by the related literature references.

The integration of these detection schemes into a single device capable of simultaneously interfacing with in vitro living cells while detecting in real-time their exposure to ionizing radiation represents a novel concept and thus an innovative experimental tool, therefore enabling the implementation of an entirely new class of micro-radiobiological experiments.

A demonstrative example of the application of these detectors consisted in the recent investigation of the stimulation of neurotransmitters secretion induced by X-ray photons (Picollo et al., 2020). In this study, the correlation between exposure to an X-ray nano-beam and the increase of the neurosecretion activity of in vitro PC12 cell line was successfully demonstrated at the single-cell level by employing a sub-micrometric X-ray beam from a synchrotron source, but without providing a comprehensive and systematic description of the phenomenon.

In this paper, we report on the fabrication and systematic characterization of diamond-based sensors developed to simultaneously carry out both of the above-described types of measurements. The detection scheme implemented for the investigation of cellular activity is an amperometric one. This amperometric technique allows a fast and real-time recording of an electrical signal due to the collection of electrons deriving from the oxidation of the secreted molecules (dopamine in our case) and therefore identifying the quantal exocytotic events at a single-cell level (Fig. 1 of Supporting Information schematically reports the detection scheme). The released neurotransmitters, when in contact with the electrode surface, are oxidized and produce an amperometric spike current of 20–100 pA lasting a few ms. Due to the excellent temporal resolution of this technique (i.e. sub-millisecond time scale), the distinct kinetic phases of the amperometric event (i.e. the measured spike) can be identified, and the vesicular content of the secretory granule can be quantified (see Fig. 1SI).

Other approaches, such as fluorimetric analysis (Angleson and Betz, 1997) and patch-clamp (Angleson and Betz, 1997; Gillis, 1995; Lindau and Neher, 1988) require complex instrumentation that cannot allow their application in concurrence with radiobiology experiments and do not provide a direct measurement of the released molecules, but only other indirect effects associated with the variation of specific environmental parameters (e.g. fluorescence intensity, cell membrane capacity).

The proper performance of amperometry technique with our diamond biosensor was already validated, in our previous publications (Picollo et al., 2013, 2016b) in terms of neurotransmitters detection capability and identification of temporal fingerprint of the signals, in comparison with single Carbon Fiber Electrodes (CFE), since no multi-electrode arrays for amperometric analysis can be found in commerce. In the same papers we demonstrated the reproducibility over several devices and multiple experiments. An exemplary dataset is reported in Table 1SI of Supporting Information. Aside from filling this technological gap, our device represents even a further step in the field, with remarkable potential in the real-time simultaneous evaluation of the biological effect of radiation and the locally delivered dose.

The sensitivity of the technique was demonstrated by means of cyclic voltammetric measurements. The ionizing radiation detection capability was tested using both alpha particles and X-ray photons, with the latter delivered from a broad beam. Finally, a radiobiological experiment demonstrating the possibility to real-time recording the effect on the dopamine release from PC12 cell culture induced by ionizing radiation is reported.

## 2. Materials and methods

### 2.1. Device microfabrication

The diamond-based sensors were fabricated using Chemical Vapour Deposited single-crystal diamond substrates 4 × 4 $mm^2$ in size and 60 μm in thickness (provided by Applied Diamond, Inc.). These substrates are classified as type IIa detector grade, being characterized by a concentration of nitrogen and boron both lower than 1 ppb.

Deep Ion Beam Lithography (DIBL) technique was employed, as it represents the ideal fabrication approach to create the embedded

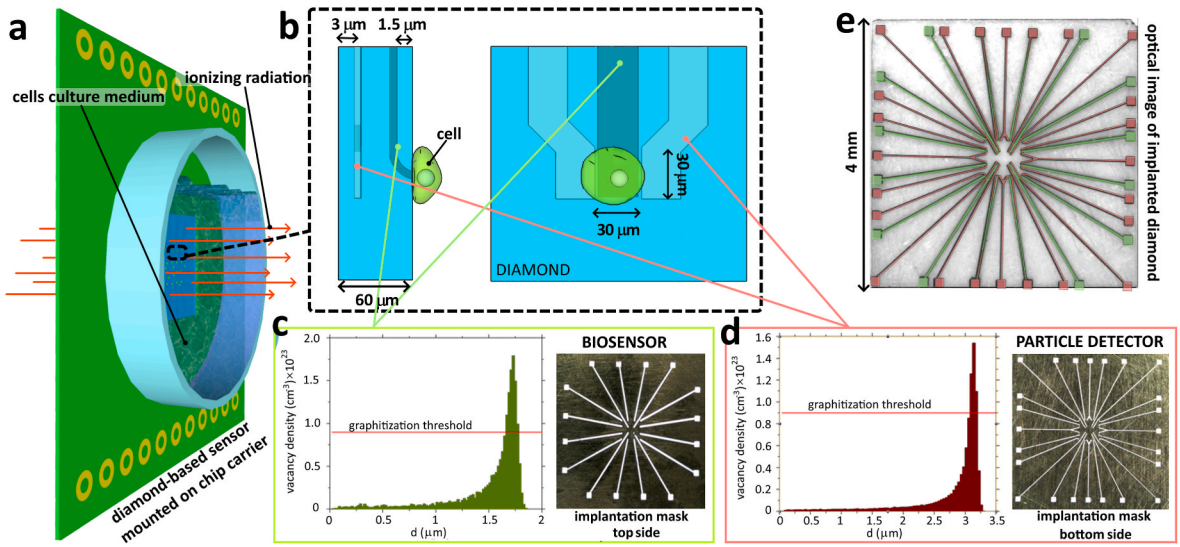


**Fig. 1.** a) Schematic representation of the diamond sensor mounted on the chip carriers. b) Schematic of the active region of one of the 16 independent channels. As can be observed from the sketch, the dosimetric electrodes are arranged so as to create a uniform electric field within the biosensing channels active region. c) Ion beam implantation conditions for the fabrication of the biosensing electrodes: SRIM (Ziegler et al., 2010) Monte Carlo simulation of the vacancy density profile induced by 1 MeV $He^+$ ion irradiation at a $1 \times 10^{17}$ $cm^{-2}$ fluence, and corresponding implantation collimator. d) Ion beam implantation condition for the fabrication of the dosimetric electrodes: SRIM simulation of the vacancy density profile induced by 1.8 MeV $He^+$ ion irradiation at $1 \times 10^{17}$ $cm^{-2}$ fluence, and the corresponding implantation collimator. e) Optical micrograph of the diamond substrate of the two implantation processes. The different types of graphitic electrodes are colour-highlighted in order to distinguish the biosensing (green) from the dosimetric (red) ones.

graphitic micro-channels by inducing the formation of graphitic layers at a well-defined and localized depth with respect to the surface (Bernardi et al., 2015; Picollo et al., 2010). Structural defects inside the diamond crystal are caused by the nuclear interaction between the accelerated ions and the carbon atoms and result in substantial changes in the chemical, structural and electrical properties of the target. At the end of the range of the ions (i.e. in correspondence of the so-called Bragg peak), the $sp^3$ diamond phase is converted into a network of $sp^2$–bonded carbon (Fig. 1c and 1d). In these regions, at high irradiation fluences, the concentration of structural defects exceeds the graphitization threshold ($5 \times 10^{22} \div 9 \times 10^{22}$ vacancies $cm^{-3}$ (Battiato et al., 2016; Hickey et al., 2009; Khmelnitsky et al., 2015)), which is defined as the critical damage density above which the loss of the diamond structure and the formation of amorphous carbon takes place (Gippius et al., 1999; Olivero et al., 2006; Uzansaguy et al., 1995). Below the graphitization threshold, Frenkel's defects are created in the first approximation.

A high-temperature thermal treatment in vacuum ($10^{-7}$ mbar) at 950 °C for 2 h was performed, allowing the permanent phase transition from amorphous $sp^2$ carbon to polycrystalline graphite and the restoration of the diamond structure in the regions with Frenkel's defects.

Ion implantations were performed at the AN2000 accelerator of the Legnaro National Laboratories of the Italian Institute of Nuclear Physics (LNL-INFN) using a collimated 1 MeV $He^+$ ion beam delivering a fluence of $1 \times 10^{17}$ $cm^{-2}$. These irradiations followed by the above-mentioned annealing process resulted in the formation of 16 biosensing micro-channels (~20 µm in width, 1.4 ÷ 1.9 mm in length and ~250 nm thick) at a depth of ~1 µm. Complementarily, irradiation with a collimated 1.8 MeV $He^+$ beam at the same fluence on the opposite facet of the sample leads to the formation of the dosimetric microchannels, characterized by similar dimensions, but localized at a depth of ~3 µm below the irradiated surface. Their geometry is designed in order to associate two electrodes (bias and ground) in correspondence with the active area of each biosensing electrode, thus realizing a region with a strong and uniform electric field that guarantees a complete particles-detection, as it will be shown in more detail.

Fig. 1c and d shows the two employed collimators (manufactured by Kirana S.r.l.) that, following a proper alignment with an accuracy in the positioning of a few micrometres, defined the geometries of the biosensing and dosimetric electrodes, respectively. As observable in the scheme of Fig. 1e, the dosimetric micro-channels are 24: 16 channels are single-ended, representing the measuring electrodes for each biosensing electrode, while the other 8 channels are double-ended electrodes, each forming the ground electrode for two biosensing regions at the same time.

Focused Ion Beam (FIB) micromachining was successively performed to expose the buried graphitic paths to the diamond surface, either (in the case of the biosensing electrodes only) for their direct contacting with the plated cells on the substrate, for electrical bonding with the front-end electronics. It is worth noting that only the end-points of the dosimetric electrodes in the periphery of the device were surface-exposed since their end-points in the centre of the sensor are devoted to particle detection occurring in the sub-surface regions corresponding to the localization of the plated cell (see Fig. 1b).

Following ion irradiation and thermal annealing, the micro-fabricated diamond substrates are assembled with two carriers, which allow interfacing both the biosensing channels from one side and the dosimetric channels on the other one to the front-end electronics. The mounted device is schematically shown in Fig. 1a.

### 2.2. Signal processing

A custom electronics board was designed to simultaneously collect and process biological and the passage of ionizing particles (Fig. 2SI). In the following, "dosimetric signal" is to be intended as the induced charge signals emerging from the buried electrodes acting as particle detectors. For the acquisition of the exocytotic signals, a LabView-controlled chain composed of a set of 16 low-noise transimpedance amplifiers and an ADC converter (National Instrument DAQ NI USB-6289) was employed. The signals were recorded at a sampling frequency of 25 kHz and filtered by a Bessel low-pass filter with a cut-off frequency of 4 kHz. Instead, for the acquisition of the dosimetric signals, two Time Of Flight Front-End Electronics (TOFFEE) chips were employed, which pre-amplify and discriminate the ionization-induced signals (Staiano et al., 2017). These chips consist of ASIC front-ends with 8 independent channels, each composed of a transimpedance amplifier, a single threshold discriminator, a signal-stretcher and an

LVDS (Low Voltage Differentil Signal) driver. The output signal is a step-like wave, whose leading edge is defined as the Time Of Arrival (TOA) of the signal, while the width is defined as the Time Over Threshold (ToT). The latter parameter holds information about the charge collected by the sensor, which is related to the energy deposited in its sensitive region.

The 16 dosimetric measuring electrodes were connected to the TOFFEE chips while the other corresponding polarizing electrodes were connected to the bias source. The voltage difference applied between the sensing and polarizing electrodes of each pair allows the generation of a strong localized electric field across a region of the diamond substrate located directly below the biosensing electrode. In this way, it is possible to locally detect the radiation that specifically hit the region corresponding to the cultured cell whose biological activity is monitored by the corresponding biosensing electrode. The number of generated electron-hole pairs is determined by the energy transferred to the material, which in diamond is 13.3 eV per pair (Zou et al., 2020).

During the experiments, each TOFFEE channel threshold was set at 470 mV, in order to cut-off the noise during data collection.

### 2.3. Radioactive sources

#### 2.3.1. X-ray source

A 150 kV Microfocus X-Ray Source (Hamamatsu L8121-03) equipped with a tungsten anode was used to qualitatively assess the response of the diamond device to X-ray exposure. The source has a tube voltage ranging from 40 kV to 150 kV and a tube current ranging from 0 μA to 500 μA. The radiation cone has an angle of approximately 43° and the source can operate with a small (7 μm), middle (20 μm) or large (50 μm) electron spot size. The X-ray source has a 200 μm thick beryllium output window.

#### 2.3.2. Alpha particle source

A $^{241}$Am source with a nominal activity of 9.775 kBq, that emits α-particles of 5.47 MeV, whose energy is completely absorbed into the diamond sample, and γ-particles of 60 keV was employed to perform radiation detection tests. Since the range in air of α-particles is a few centimetres, during the experiments the source was placed at a distance smaller than 1 cm from the diamond sample.

### 2.4. PC12 preparation

PC12 cell is a cell line derived from pheochromocytoma of the rat adrenal medulla. The diamond-based sensors were coated with collagen type I (Sigma-Aldrich) used as a substrate for cell adhesion and cells are maintained in an incubator with RPMI-1640 (Invitrogen) medium containing 10% horse serum (Invitrogen), 5% fetal bovine serum (Invitrogen) and 2% antibiotic/antimitotic (pen/strep Invitrogen), at a temperature of 37 °C in a 5% $CO_2$ atmosphere. The experiments are performed 3/4 days after culturing at room temperature (Tomagra et al., 2019b).

## 3. Results and discussion

In the following, the results of electrochemical tests are shown, as well as the functional characterization of the response to the ionizing radiation of the diamond-based detector by employing both alpha particles and X-rays. Finally, a demonstrative application of these sensors for a specific case study is presented, by reporting the results of the investigation of the effect of X-ray irradiation on the spontaneous exocytotic activity of PC12 cells.

### 3.1. Electrical and electrochemical characterization

The electrical characterization of the biosensing electrodes was performed to assess the effectiveness of the fabrication process (i.e.: full graphitization of the channels, effective electrical contact, etc.). The current-voltage characteristics of the graphitic microchannels were measured in a two-terminal configuration by sweeping the voltage between −3 V and +3 V at 0.1 V steps, showing a linear ohmic trend (Fig. 2a). The resistivity obtained by averaging values measured from 15 electrodes is (1.9 ± 0.3) mΩ cm, which is compatible with values reported for polycrystalline graphite, i.e. $\rho_g = (1 \div 4)$ mΩ cm, as well as those reported from similar structures in previous studies (Olivero et al., 2009; Picollo et al., 2012). It is worth noting that one of the 16 electrodes is characterized by a significantly higher resistance value, which is ascribable to a failure in the lithographic process.

To confirm the capability of the devices for the detection of dopamine, cyclic voltammetry was carried out in physiological saline solutions, (Tyrode solution, containing 128 mM of NaCl, 2 mM of $MgCl_2$, 10 mM of glucose, 10 mM of HEPES, 10 mM of $CaCl_2$ and 4 mM of KCl) and in Tyrode solution with the addition of 75 μM of dopamine. The measurements were performed by applying a triangular voltage waveform and sweeping the electrode bias between −0.5 V and +1.2 V, with a scan rate of 10 mV $s^{-1}$; during measurement, the solution was grounded with an Ag/AgCl reference electrode. Fig. 2b shows the voltammograms of four representative electrodes. The curves recorded from the Tyrode solution are characterized by a voltage interval characterized by a low current (−0.5 V ÷ 1 V), which is usually referred to as "water window", while a steep current increase at bias values larger than 1 V is due to water oxidation. After the perfusion of the dopamine into the solution, the acquired voltammograms exhibit a shoulder at 0.5 V–0.8 V, which is directly ascribable to the oxidation of dopamine, consistently with previous reports (Venton and Wightman, 2003). In order to maximize the signal-to-noise ratio, a 650 mV bias was applied during the following amperometric measurements.

The sensitivity of the diamond-based multi-electrode array in terms of dopamine detection using amperometric measurements was assessed in previous works (Picollo et al., 2016a; Tomagra et al., 2019a). In particular, acquired data showed a linear dependence between the measured amperometric current and the concentration of neurotransmitters solution (namely, dopamine and adrenaline) resulting in an estimated limit-of-detection (LOD) value of ~1 μM (see Fig. 3SI).

It is worth remarking that the exocytosis processes are characterized by a concentration of secreted molecules of (148 ± 8) mM (Anderson et al., 1999), which is 5 orders of magnitude higher with respect to our LOD.

### 3.2. α-particles detection

A $^{241}$Am α-particle source was placed at a distance of ~7.5 mm from the bottom of the sensor (see Fig. 2SI panel b), with the purpose of testing its capability of detecting particles depositing their entire energy within a 13.5 μm thickness, which is well within the active region of each "pixel" of the detector.

Data were acquired by setting different bias voltages, to identify the lower $V_{bias}$ value guaranteeing an optimal signal detection, without perturbing the biosensing recording. The bias was set at 10 V, 20 V and 30 V, although previous studies demonstrated that 100% of charge collection efficiency was obtained using 80 V–100 V (Forneris et al., 2014) for graphitic electrodes embedded in diamond in a similar geometry (i.e. ~30 μm electrode distance).

Fig. 3a shows the histograms of the distributions of the charge induced from the alpha-particles, recorded from a representative active region at different biases. These values were normalized with respect to the total number of detected events in order to better compare the different bias configurations.

For all the adopted $V_{bias}$ values, these energy distributions present two identifiable features:

- A tail located between 0 fC and 10 fC, which is ascribable to the particles impinging the detector across an area that is outside, but

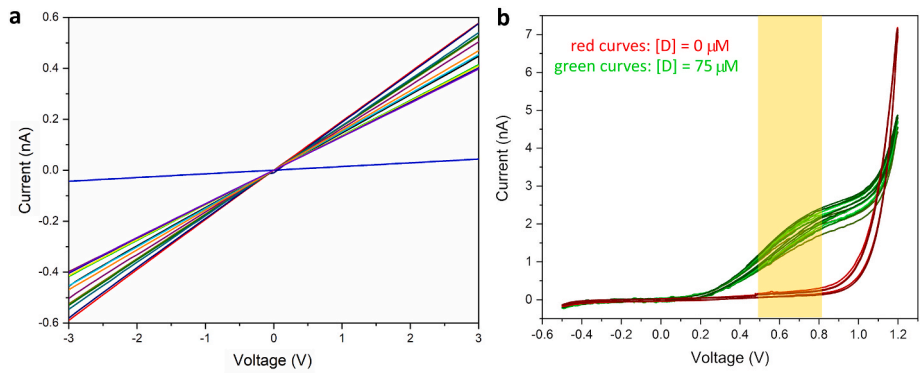


**Fig. 2.** a) I–V characterization of the 16 biosensing electrodes; blue curve presenting higher resistance is attributed to a failure in the fabrication process of one of the sixteen electrodes. b) Cyclic voltammograms were recorded from four representative channels in a saline solution, both with and without the addition of dopamine [75 μM]. The dopamine oxidation region is highlighted in yellow.

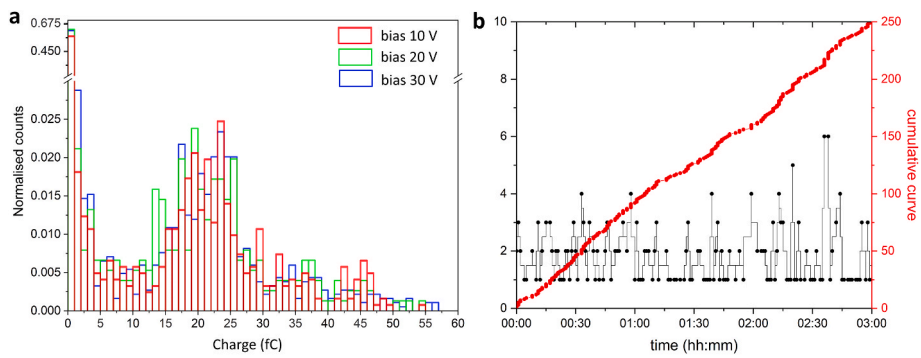


**Fig. 3.** a) Statistical distribution of the charge of the detected alpha particles normalized with respect to the total detected events. b) Chronogram of the number of detected events in the >10 fC window and the related cumulative curve setting a bias voltage of 10 V.

sufficiently close to the active region resulting in a partial charge collection. These events can be easily identified on a spectral basis and thus discarded during data analysis.

- The signals detected with an induced charge higher then 10 fC are related to interaction generated by the ions crossing the sensitive area of the device, representing the events of interest.

Since the complete collection of the induced charge from 5.47 MeV α-particle in diamond correspond to a charge of about 65 fC, the modal charge collection efficiency of this device is around 30%.

Fig. 3b reports the chronogram of the number of signals collected with a 10 V bias voltage, upon the exclusion of events at low (i.e. < 10 fC) energies, and the related cumulative curve corresponding to the integral of the detected events during the measurement time.

Taking into consideration the activity of the source (a = 9.775 kBq) and the solid angle of the emitted alpha particles impinging the active area (A ≃ 30 μm × 60 μm) of the selected representative pixel, it is possible to evaluate the maximum number of detectable particles by the following equation

$$\#_{particles\ on\ active\ area} = \frac{a}{4\pi\, d^2} A\, t = \frac{9.775\ kBq}{4\pi\ (7.5{\cdot}7.5)\ mm^2}\ (30 \cdot 60)\ \mu m^2\ 10800\ s = 269$$

where $d$ is the distance between source and detector and $t$ is the acquisition time; obtaining ~270 detected events. Comparing this expected number of events with the detected ones (Fig. 3b red curve) it is possible to confirm the capability of the diamond-sensor to detect single particles having a counting efficiency close to 93%.

The device showed a comparable efficiency in the particle detection for all the set biases, and therefore during the subsequent measurements the lower voltage (10 V) was employed in order to minimize the potential interferences with biosensing recordings.

### 3.3. X-ray beam detection

X-ray detection tests were performed using a microfocus source covering completely the sensor surface to investigate the performance of the device when crossed by photons.

The X-ray tube current was set to 500 μA while the measurements were carried out by varying the acceleration voltage across the following values: 40 kV, 80 kV, 100 kV, 120 kV and 150 kV, integrating the signal for 10 min in each case. The sensor was located at a distance of 3.7 cm from the source.

The histograms of the ToT values of the detected signals obtained by setting different tube voltages are reported in Fig. 4 and compared with the emission spectra simulated with the SpekCalc software (Poludniowski et al., 2009) by setting the proper source parameters. These simulations were performed taking into account the X-ray attenuation ascribable to both the beryllium window (0.2 mm) and air (3.7 cm). Differently from the characterization with the alpha particles, the ToT values are related to a partial energy deposition and are therefore not indicative of the energy of the photon. In the following, all the comments are reported considering the ToT values since offering a clearer distribution of the features of the data with respect to using the charge values (Fig. 4).

The spectrum of the X-ray radiation emitted using tube acceleration voltages of 40 kV and 80 kV are mainly characterized by the bremsstrahlung component since the energies of the $K_\alpha$ and $K_\beta$ spectral lines of the tungsten target are 57.420 keV and 66.952 keV (Bearden, 1967), respectively, and therefore their emission is not (or poorly) stimulated. Consequently, the ToT distribution collected by the sensors exhibits a peak at 3.2 ns with a full-width half-maximum of 1.5 ns corresponding to

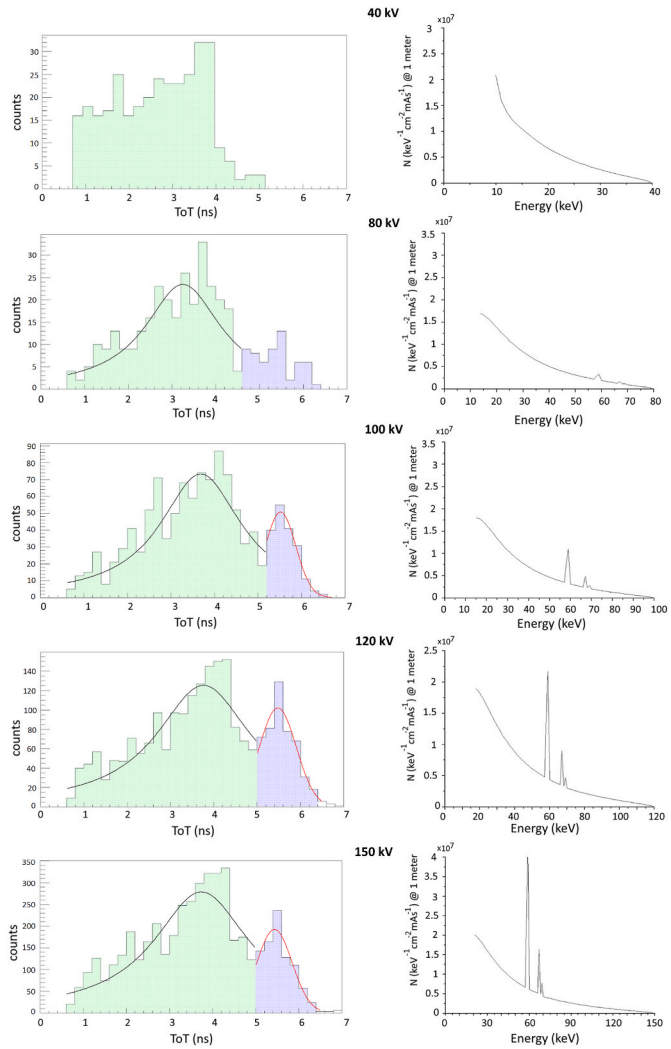


**Fig. 4.** First column: statistical distribution of the ToT values of the detected signals, as collected by varying the acceleration voltage of the X-ray source. Second column: simulated X-ray emission spectra as resulting from SpecCalc software by setting the employed experimental conditions.

the peak of the bremsstrahlung emission, while a small increase in the count rate is barely visible with respect to the background (K peaks) at higher ToT values (~5.5 ns) only under 80 kV acceleration voltage.

At higher acceleration voltages, the spectral contribution from the characteristic X-ray emission becomes more significant, and it appears in the ToT distribution as a peak at 5.5 ns which is ascribable to the convolution of the $K_\alpha$ and $K_\beta$ spectral lines while the maximum of the bremsstrahlung radiation, as expected, is slightly shifting at higher ToT values (i.e. from 3.2 ns to 3.8 ns) as well as becoming more intense.

### *3.4. Biosensing measurements from a PC12 cell line during X-ray irradiation*

After the functional characterization, the diamond-based sensors were employed to investigate the effects induced by X-ray irradiation on the physiological activity of cultured cells. The acceleration voltage was set to 40 kV, thus resulting in a emission spectrum with a mean energy value of 17 keV, which corresponds to the monochromatic syncrothron beam used in (Picollo et al., 2020).

These preliminary and proof-of-concept experiments were focused on the recording of dopamine release from the PC12 cell line during the detection of the deposited dose, reaching a value comprised between 1 Gy and 5 Gy.

The PC12 cell line was selected as exemplary, since it is widely employed to study the regulatory principles of the exocytosis in neurons, which share with them both the secretory mechanism and the released molecules (namely dopamine) (Westerink and Ewing, 2007). For sake of example, it is possible to use the device to measure secretory events also from cultured neuronal cells networks detecting the release of catecholamines (Picollo et al., 2020), tissues line adrenal gland cells detecting adrenaline (Picollo et al., 2016a), pancreatic cells detecting insulin and platelets detecting dopamine. Therefore, these cells represent a fully characterized standard biological sample. PC12 cells were directly plated over the diamond sensor surface and maintained in culture for 3/4 days. The growing chamber on which the PC12 are cultured hosts a large number of cells (cell density after plating: $1 \times 10^6$ cells cm$^{-2}$, doubling time of 92 h, 3 day in vitro before the measurements), but the size of the active region of the graphitic micro-electrodes (roughly 20 μm in diameters), which is similar to that of the investigated cells, guarantees that the recorded signals are associated with the local release of dopamine molecules from a single cells. Infrequently, more than one cell can grow sharing the active region of the same electrodes, but these inconveniences are negligible due to the high statistic that multi electrode array sensors can collect.

After the mentioned period of maturation, the cells show a spontaneous exocytic activity as already reported in (Tomagra et al., 2019b). Quantal exocytotic events correspond to the release of oxidizable neurotransmitters docked in vesicles present in the cells into the extracellular medium and the evolution along the time of this process is regulated by complex physiological pathways characteristic of the biological system under exam (see schematic shown in Fig. 1SI).

With the employment of the biosensing function of the developed device, the spontaneous activity of PC12 cells was monitored for 800 s.

The 16 electrodes were held at a constant potential of +650 mV relative to the Ag/AgCl reference electrode in the culture medium, which represents the optimal value for the detection of dopamine as identified by means of the cyclic voltammetry.

Fig. 5a shows a typical chronoamperogram corresponding to non-irradiation conditions, in which are distinguishable the amperometric spikes (single exocytic events) overhead the noise band. The time behaviour of the mean frequency of the detected spikes, obtained averaging the signals from 5 electrodes, was evaluated considering timing windows of 30 s and it is reported in Fig. 5b. The frequency of exocytic events presents a slowly increasing trend which reaches a maximum of 0.8 Hz after 270 s followed by a faster decrease and a substantial interruption of the activity (>0.1 Hz) after 400 s.

During the irradiation experiments, the biosensor was placed vertically in front of the X-ray source at a distance of ~6 cm. Care was taken to align the radiation emission spot with the centre of the diamond biosensor and consequently with the biological sample.

Initially, spontaneous secretory events were acquired as a control dataset, therefore, maintaining the above-described configuration, the exocytotic activity was monitored simultaneously with the irradiation of the PC12 cells with X-ray photons (acceleration voltage 40 kV and cathodic current 200 μA).

Fig. 6 shows the chronoamperogram recorded from a representative electrode.

By monitoring the frequency of the detected amperometric peaks before and during the irradiation (f= (0.44 ± 0.13) Hz and f= (0.97 ± 0.04) Hz, respectively) an increment of 220% of the exocytotic activity is observable (the effect is statistically significant with $p > 0.01$). This increment is measured by comparing the frequency of the signals detected from 30 s before the start of the RX exposure with those evaluated during the first 30 s of irradiation which corresponds to the delivery of a dose of (1.0 ± 0.1) Gy. Due to its rapid variation, this effect is ascribable to the photon exposure and not to the spontaneous activity trend which would require a longer time to reach such intensity (Fig. 5).

This measurement, which is in agreement with those reported in

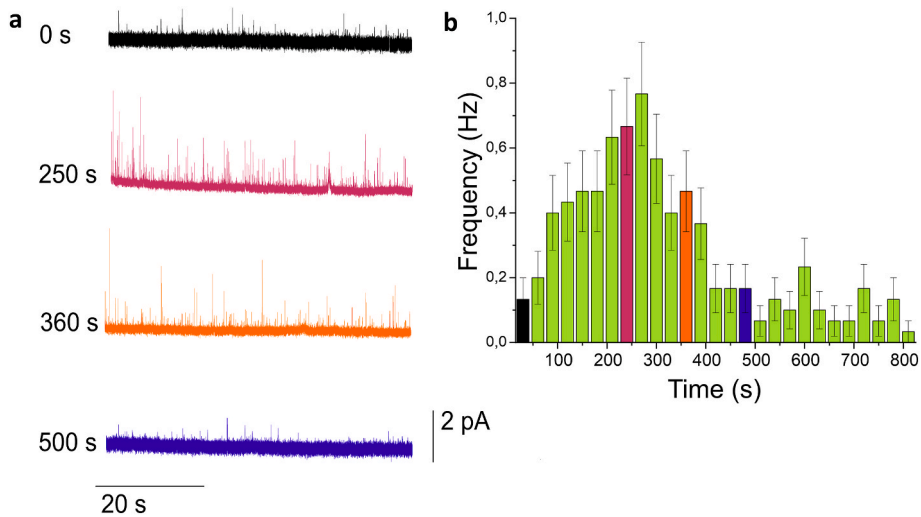


**Fig. 5.** a) Chronoamperogram from a representative electrode of the spontaneous exocytotic activity of a PC12 cell at different times (0 s, 250 s, 360 s and 500 s) b) Distribution of the frequency of the detected "amperometric spikes" events. The coloured bars are related to the chronoamperogram of panel a).

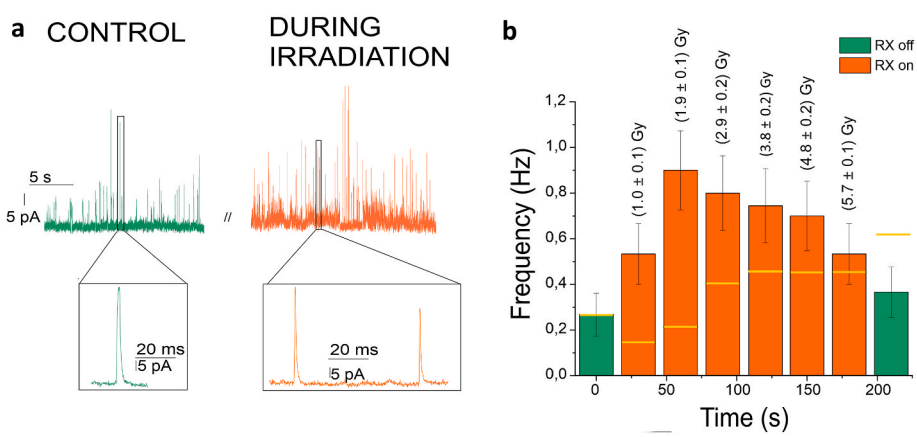


**Fig. 6.** a) Chronoamperogram from a representative electrode of the spontaneous exocytotic activity of a PC12 cell before (control) and during X-ray irradiation. Measurements parameters: potential applied to the working electrodes +650 mV; sampling frequency 25 kHz, filter frequency 4 kHz (Bassel filter). The inset reports the magnification of a small portion of the amperometric recording showing the characteristic shape of exocytotic peaks. b) Distribution of the frequency of the detected exocytotic events: red bars are associated with the signal recorded during the exposure of the cell to the X-rays with reported the cumulated dose. Blue dashed lines correspond to the data shown in Fig. 5 for related time.

(Picollo et al., 2020) obtained at a synchrotron facility, represents the first evidence of the possibility to monitor in real-time the variation of cellular activity during X-ray irradiation using a tabletop set-up, opening the way to study these phenomena in every laboratory.

## 4. Conclusions

At present, radiotherapy represents a powerful technique, but it is affected by substantial side effects ascribable to the perturbation of healthy cells which are not strictly related to their death, but mainly to the modification of their physiological activity. Several studies try to describe and understand these. This work directly addresses this substantial topic, thanks to the development of a device which is capable of simultaneously measuring the irradiation dose and the biological effect, in real-time and with a high temporal and spatial resolution.

Innovative artificial-diamond based sensors have been described and characterized to perform radiobiological experiments detecting simultaneously the ionizing radiation and the exocytotic activity from a network of cells. The graphitic channels implanted into diamond through the Ion Beam Lithography act as electrodes for the collection of the signals induced by the ionizing radiation as well as for the detection by amperometry of the molecules secreted from single cells.

A demonstrative application of a case study was performed proving the applicability of these devices for in vitro experiments: the modulation of dopamine release from PC12 cells triggered by X-rays was observed using a standard Roentgen tube, confirming a similar result obtained at a synchrotron facility reported in (Picollo et al., 2020). Further investigation combining these sensors with pharmacological treatments (inhibition or stimulation of spontaneous exocytosis) can clarify the biological pathways activated by the ionizing radiation which could have a potential impact on the understanding of undesired and still unknown secondary effects observed during radiotherapy cancer treatments.

The potentiality of these sensors can be also extended by implementing a supplementary detection scheme (as potentiometry) allowing the investigation of the effects induced on electrical signals during cells exposition to ionizing radiation, like neuronal or cardiac action potentials (Tomagra et al., 2019a).

## CRediT authorship contribution statement

**Giulia Tomagra:** Investigation, Writing – review & editing. **Giulia Peroni:** Writing – original draft, Writing – review & editing. **Pietro Aprà:** Investigation, Writing – review & editing. **Valentina Bonino:** Formal analysis, Writing – review & editing. **Matteo Campostrini:** Formal analysis, Writing – review & editing. **Valentina Carabelli:** Supervision, Writing – review & editing. **Cecilia Collà Ruvolo:** Investigation, Writing – review & editing. **Alessandro Lo Giudice:** Resources, Writing – review & editing. **Laura Guidorzi:** Resources, Writing – review & editing. **Lorenzo Mino:** Visualization, Writing – review &

editing. **Paolo Olivero:** Supervision, Writing – review & editing. **Luca Pacher:** Investigation, Writing – review & editing. **Fabio Picariello:** Software, Writing – review & editing. **Alessandro Re:** Resources, Writing – review & editing. **Valentino Rigato:** Supervision, Writing – review & editing. **Marco Truccato:** Supervision, Writing – review & editing. **Veronica Varzi:** Formal analysis, Writing – review & editing. **Ettore Vittone:** Conceptualization, Writing – review & editing. **Federico Picollo:** Writing – original draft, Project administration, Funding acquisition, Writing – review & editing.

## Declaration of competing interest

The authors declare that they have no known competing financial interests or personal relationships that could have appeared to influence the work reported in this paper.

## Data availability

Data will be made available on request.

## Acknowledgements

The authors thank Nicolò Cartiglia (National Institute for Nuclear Physics (INFN), Section of Torino, Italy) for the useful support provided for the ionizing radiation detection measure, Giorgio Cotto (Physic Department, University of Torino, Italy) for the suggestion for the instrumentation interfacing with PC and Marco Mignone ( National Institute for Nuclear Physics (INFN), Section of Torino, Italy) for the realization of the front-end electronic. This work was supported by: the "RESOLVE" project funded by the National Institute for Nuclear Physics (INFN); "BiophysiX" project funded by the CRT Foundation, "QuantDia" project funded by the Italian Ministry for Education, University and Research (MIUR)within the "FISR 2019" program and the Grant "Departments of Excellence" (L. 232/2016), funded by the Italian Ministry of Education, University and Research (MIUR).

## Appendix A. Supplementary data

Supplementary data to this article can be found online at https://doi.org/10.1016/j.bios.2022.114876.

## References

Anderson, B.B., Zerby, S.E., Ewing, A.G., 1999. Calculation of transmitter concentration in individual PC12 cell vesicles with electrochemical data and a distribution of vesicle size obtained by electron microscopy. J. Neurosci. Methods 88, 163–170. https://doi.org/10.1016/S0165-0270(99)00023-0.

Angleson, J.K., Betz, W.J., 1997. Monitoring secretion in real time: capacitance, amperometry and fluorescence compared. Trends Neurosci. 20, 281–287. https://doi.org/10.1016/S0166-2236(97)01083-7.

Ariano, P., Baldelli, P., Carbone, E., Gilardino, a., Lo Giudice, a., Lovisolo, D., Manfredotti, C., Novara, M., Sternschulte, H., Vittone, E., 2005. Cellular adhesion and neuronal excitability on functionalised diamond surfaces. Diam. Relat. Mater. 14, 669–674. https://doi.org/10.1016/j.diamond.2004.11.021.

Battiato, A., Lorusso, M., Bernardi, E., Picollo, F., Bosia, F., Ugues, D., Zelferino, A., Damin, A., Baima, J., Pugno, N.M., Ambrosio, E.P., Olivero, P., 2016. Softening the ultra-stiff: controlled variation of Young's modulus in single-crystal diamond by ion implantation. Acta Mater. 116, 95–103. https://doi.org/10.1016/j.actamat.2016.06.019.

Bearden, J.A., 1967. X-ray wavelengths. Rev. Mod. Phys. 39, 78–124. https://doi.org/10.1103/RevModPhys.39.78.

Bernardi, E., Battiato, A., Olivero, P., Picollo, F., Vittone, E., 2015. Kelvin probe characterization of buried graphitic microchannels in single-crystal diamond. J. Appl. Phys. 117 https://doi.org/10.1063/1.4905425.

Bloomer, C., Newton, M.E., Rehm, G., Salter, P.S., 2020. A single-crystal diamond X-ray pixel detector with embedded graphitic electrodes. J. Synchrotron Radiat. 27, 599–607. https://doi.org/10.1107/S160057752000140X.

Carabelli, V., Marcantoni, A., Picollo, F., Battiato, A., Bernardi, E., Pasquarelli, A., Olivero, P., Carbone, E., 2017. Planar diamond-based multiarrays to monitor neurotransmitter release and action potential firing: new perspectives in cellular neuroscience. ACS Chem. Neurosci. 8, 252–264. https://doi.org/10.1021/acschemneuro.6b00328.

Carlisle, J.A., 2004. Precious biosensors. Nat. Mater. 3, 668–669. https://doi.org/10.1038/nmat1225.

Durante, M., Brauer-Krisch, E., Hill, M., 2017. Faster and safer? FLASH ultra-high dose rate in radiotherapy. Br. J. Radiol., 20170628 https://doi.org/10.1259/bjr.20170628.

Fan, B., Rusinek, C.A., Thompson, C.H., Setien, M., Guo, Y., Rechenberg, R., Gong, Y., Weber, A.J., Becker, M.F., Purcell, E., Li, W., 2020. Flexible, diamond-based microelectrodes fabricated using the diamond growth side for neural sensing. Microsyst. Nanoeng. 6, 42. https://doi.org/10.1038/s41378-020-0155-1.

Favaudon, V., Caplier, L., Monceau, V., Pouzoulet, F., Sayarath, M., Fouillade, C., Poupon, M.-F., Brito, I., Hupé, P., Bourhis, J., Hall, J., Fontaine, J.-J., Vozenin, M.-C., 2014. Ultrahigh dose-rate FLASH irradiation increases the differential response between normal and tumor tissue in mice. Sci. Transl. Med. 6 https://doi.org/10.1126/scitranslmed.3008973.

Forneris, J., Battiato, A., Gatto Monticone, D., Picollo, F., Amato, G., Boarino, L., Brida, G., Degiovanni, I.P.P., Enrico, E., Genovese, M., Moreva, E., Traina, P., Verona, C., Verona Rinati, G., Olivero, P., 2015. Electroluminescence from a diamond device with ion-beam-micromachined buried graphitic electrodes. Nucl. Instrum. Methods Phys. Res. Sect. B Beam Interact. Mater. Atoms 348, 187–190. https://doi.org/10.1016/j.nimb.2014.12.036.

Forneris, J., Grilj, V., Jakšić, M., Lo Giudice, a., Olivero, P., Picollo, F., Skukan, N., Verona, C., Verona-Rinati, G., Vittone, E., 2013. IBIC characterization of an ion-beam-micromachined multi-electrode diamond detector. Nucl. Instrum. Methods Phys. Res. Sect. B Beam Interact. Mater. Atoms 306, 181–185. https://doi.org/10.1016/j.nimb.2012.12.056.

Forneris, Jacopo, Grilj, V., Jakšić, M., Olivero, P., Picollo, F., Skukan, N., Verona, C., Verona-Rinati, G., Vittone, E., 2013. Measurement and modelling of anomalous polarity pulses in a multi-electrode diamond detector. EPL (Europhysics Lett. 104, 28005 https://doi.org/10.1209/0295-5075/104/28005.

Forneris, J., Lo Giudice, A., Olivero, P., Picollo, F., Re, A., Marinelli, M., Pompili, F., Verona, C., Rinati, G.V., Benetti, M., Cannata, D., Pietrantonio, F., Di Verona Rinati, G., Benetti, M., Cannata, D., Di Pietrantonio, F., Rinati, G.V., Benetti, M., Cannata, D., Pietrantonio, F., Di Verona Rinati, G., Benetti, M., Cannata, D., Di Pietrantonio, F., 2014. A 3-dimensional interdigitated electrode geometry for the enhancement of charge collection efficiency in diamond detectors. EPL (Europhysics Lett. 108, 18001 https://doi.org/10.1209/0295-5075/108/18001.

Gillis, K.D., 1995. Techniques for membrane capacitance measurements. In: Single-Channel Recording. Springer US, Boston, MA, pp. 155–198. https://doi.org/10.1007/978-1-4419-1229-9_7.

Gippius, A.A.A., Khmelnitskiy, R.A.R., Dravin, V.A., Tkachenko, S.D., 1999. Formation and characterization of graphitized layers in ion-implanted diamond. Diam. Relat. Mater. 8, 1631–1634. https://doi.org/10.1016/S0925-9635(99)00047-3.

Gkoumas, S., Lohstroh, A., Sellin, P.J., 2009. Low temperature time of flight mobility measurements on synthetic single crystal diamond. Diam. Relat. Mater. 18, 1338–1342. https://doi.org/10.1016/j.diamond.2009.07.006.

Grilj, V., Skukan, N., Pomorski, M., Kada, W., Iwamoto, N., Kamiya, T., Ohshima, T., Jakšić, M., 2013. An ultra-thin diamond membrane as a transmission particle detector and vacuum window for external microbeams. Appl. Phys. Lett. 103, 243106 https://doi.org/10.1063/1.4833236.

Hébert, C., Scorsone, E., Bendali, A., Kiran, R., Cottance, M., Girard, H.A., Degardin, J., Dubus, E., Lissorgues, G., Rousseau, L., Mailley, P., Picaud, S., Bergonzo, P., 2014. Boron doped diamond biotechnology: from sensors to neurointerfaces. Faraday Discuss 172, 47–59. https://doi.org/10.1039/c4fd00040d.

Hickey, D.P., Jones, K.S., Elliman, R.G., 2009. Amorphization and graphitization of single-crystal diamond - a transmission electron microscopy study. Diam. Relat. Mater. 18, 1353–1359. https://doi.org/10.1016/j.diamond.2009.08.012.

Jansen, H., Dobos, D., Eisel, T., Pernegger, H., Eremin, V., Wermes, N., 2013. Temperature dependence of charge carrier mobility in single-crystal chemical vapour deposition diamond. J. Appl. Phys. 113 https://doi.org/10.1063/1.4802679.

Khmelnitsky, R.A., Dravin, V.A., Tal, A.A., Zavedeev, E.V., Khomich, A.A., Khomich, A. V., Alekseev, A.A., Terentiev, S.A., 2015. Damage accumulation in diamond during ion implantation. J. Mater. Res. 30, 1583–1592. https://doi.org/10.1557/jmr.2015.21.

Kopecek, M., Bacakova, L., Vacik, J., Fendrych, F., Vorlicek, V., Kratochvilova, I., Lisa, V., Van Hove, E., Mer, C., Bergonzo, P., Nesladek, M., 2008. Improved adhesion, growth and maturation of human bone-derived cells on nanocrystalline diamond films. Phys. Status Solidi 205, 2146–2153. https://doi.org/10.1002/pssa.200879729.

Krůšek, J., Dittert, I., Smejkalová, T., Kořínek, M., Gottfriedová, K., Freislebenová, H., Neuhöferová, E., Klimša, L., Sedláková, S., Taylor, A., Mortet, V., Petrák, V., Benson, V., Petráková, V., 2019. Molecular functionalization of planar nanocrystalline and porous nanostructured diamond to form an interface with newborn and adult neurons. Phys. Status Solidi 256, 1800424. https://doi.org/10.1002/pssb.201800424.

Lacombe, J., Phillips, S.L., Zenhausern, F., 2016. Microfluidics as a new tool in radiation biology. Cancer Lett. 371, 292–300. https://doi.org/10.1016/j.canlet.2015.11.033.

Lagomarsino, S., Bellini, M., Corsi, C., Gorelli, F., Parrini, G., Santoro, M., Sciortino, S., 2013. Three-dimensional diamond detectors: charge collection efficiency of graphitic electrodes. Appl. Phys. Lett. 103 https://doi.org/10.1063/1.4839555.

Lindau, M., Neher, E., 1988. Patch-clamp techniques for time-resolved capacitance measurements in single cells. Pflügers Arch. Eur. J. Physiol. 411, 137–146. https://doi.org/10.1007/BF00582306.

Macpherson, J.V., 2015. A practical guide to using boron doped diamond in electrochemical research. Phys. Chem. Chem. Phys. 17, 2935–2949. https://doi.org/10.1039/C4CP04022H.

Maybeck, V., Edgington, R., Bongrain, A., Welch, J.O., Scorsone, E., Bergonzo, P., Jackman, R.B., Offenhäusser, A., 2014. Boron-doped nanocrystalline diamond microelectrode arrays monitor cardiac action potentials. Adv. Healthc. Mater. 3, 283–289. https://doi.org/10.1002/adhm.201300062.

McDonald, M., Monaco, A., Vahidpour, F., Haenen, K., Giugliano, M., Nesladek, M., 2017. Diamond microelectrode arrays for in vitro neuronal recordings. MRS Commun 7, 683–690. https://doi.org/10.1557/mrc.2017.62.

Niklas, M., Zimmermann, F., Schlegel, J., Schwager, C., Debus, J., Jäkel, O., Abdollahi, A., Greilich, S., 2016. Registration procedure for spatial correlation of physical energy deposition of particle irradiation and cellular response utilizing cell-fluorescent ion track hybrid detectors. Phys. Med. Biol. 61, N441–N460. https://doi.org/10.1088/0031-9155/61/17/N441.

Nistor, P.A., May, P.W., Tamagnini, F., Randall, A.D., Caldwell, M.A., 2015. Long-term culture of pluripotent stem-cell-derived human neurons on diamond – a substrate for neurodegeneration research and therapy. Biomaterials 61, 139–149. https://doi.org/10.1016/j.biomaterials.2015.04.050.

Oh, A., Caylar, B., Pomorski, M., Wengler, T., 2013. A novel detector with graphitic electrodes in CVD diamond. Diam. Relat. Mater. 38, 9–13. https://doi.org/10.1016/j.diamond.2013.06.003.

Olivero, P., Amato, G., Bellotti, F., Budnyk, O., Colombo, E., Jakšić, M., Manfredotti, C., Pastuović, Ž., Picollo, F., Skukan, N., Vannoni, M., Vittone, E., 2009. Direct fabrication of three-dimensional buried conductive channels in single crystal diamond with ion microbeam induced graphitization. Diam. Relat. Mater. 18, 870–876. https://doi.org/10.1016/j.diamond.2008.10.068.

Olivero, P., Forneris, J., Jakšić, M., Pastuović, Z., Picollo, F., Skukan, N., Vittone, E., 2011. Focused ion beam fabrication and IBIC characterization of a diamond detector with buried electrodes. Nucl. Instrum. Methods Phys. Res. Sect. B Beam Interact. Mater. Atoms 269, 2340–2344. https://doi.org/10.1016/j.nimb.2011.02.021.

Olivero, P., Rubanov, S., Reichart, P., Gibson, B.C., Huntington, S.T., Rabeau, J.R., Greentree, A.D., Salzman, J., Moore, D., Jamieson, D.N., Prawer, S., 2006. Characterization of three-dimensional microstructures in single-crystal diamond. Diam. Relat. Mater. 15, 1614–1621. https://doi.org/10.1016/j.diamond.2006.01.018.

Picollo, F., Battiato, A., Bernardi, E., Marcantoni, A., Pasquarelli, A., Carbone, E., Olivero, P., Carabelli, V., 2016a. Microelectrode arrays of diamond-insulated graphitic channels for real-time detection of exocytotic events from cultured chromaffin cells and slices of adrenal glands. Anal. Chem. 88, 7493–7499. https://doi.org/10.1021/acs.analchem.5b04449.

Picollo, F., Battiato, A., Bernardi, E., Plaitano, M., Franchino, C., Gosso, S., Pasquarelli, A., Carbone, E., Olivero, P., Carabelli, V., 2016b. All-carbon multi-electrode array for real-time in vitro measurements of oxidizable neurotransmitters. Sci. Rep. 6, 20682 https://doi.org/10.1038/srep20682.

Picollo, F., Gatto Monticone, D., Olivero, P., Fairchild, B.a., Rubanov, S., Prawer, S., Vittone, E., 2012. Fabrication and electrical characterization of three-dimensional graphitic microchannels in single crystal diamond. New J. Phys. 14, 053011 https://doi.org/10.1088/1367-2630/14/5/053011.

Picollo, F., Gosso, S., Vittone, E., Pasquarelli, A., Carbone, E., Olivero, P., Carabelli, V., 2013. A new diamond biosensor with integrated graphitic microchannels for detecting quantal exocytic events from chromaffin cells. Adv. Mater. 25, 4696–4700. https://doi.org/10.1002/adma.201300710.

Picollo, F., Olivero, P., Bellotti, F., Pastuović, Ž., Skukan, N., Lo Giudice, A., Amato, G., Jakšić, M., Vittone, E., 2010. Formation of buried conductive micro-channels in single crystal diamond with MeV C and He implantation. Diam. Relat. Mater. 19, 466–469. https://doi.org/10.1016/j.diamond.2010.01.005.

Picollo, F., Tomagra, G., Bonino, V., Carabelli, V., Mino, L., Olivero, P., Pasquarelli, A., Truccato, M., 2020. Triggering neurotransmitters secretion from single cells by x-ray nanobeam irradiation. Nano Lett. 20, 3889–3894. https://doi.org/10.1021/acs.nanolett.0c01046.

Poludniowski, G., Landry, G., DeBlois, F., Evans, P.M., Verhaegen, F., 2009. SpekCalc : a program to calculate photon spectra from tungsten anode x-ray tubes. Phys. Med. Biol. 54, N433–N438. https://doi.org/10.1088/0031-9155/54/19/N01.

Pomorski, M., Berdermann, E., Ciobanu, M., Martemyianov, A., Moritz, P., Rebisz, M., Marczewska, B., 2005. Characterisation of single crystal CVD diamond particle detectors for hadron physics experiments. Phys. Status Solidi 202, 2199–2205. https://doi.org/10.1002/pssa.200561929.

Schaue, D., Mcbride, W.H., 2015. Opportunities and challenges of radiotherapy for treating cancer. Nat. Rev. Clin. Oncol. 12, 527–540. https://doi.org/10.1038/nrclinonc.2015.120.

Skukan, N., Sudić, I., Pomorski, M., Kada, W., Jakšić, M., 2019. Enhanced radiation hardness and signal recovery in thin diamond detectors. AIP Adv. 9, 025027 https://doi.org/10.1063/1.5081136.

Staiano, A., Arcidiacono, R., Boscardin, M., Betta, G.F.D., Cartiglia, N., Cenna, F., Ferrero, M., Ficorella, F., Mandurrino, M., Obertino, M., Pancheri, L., Paternoster, G., Sola, V., 2017. Development of ultra-fast silicon detectors for 4D tracking. J. Instrum. 12 https://doi.org/10.1088/1748-0221/12/12/C12012. C12012–C12012.

Steel, G.G., Mcmillan, T.J., Peacock, J.H., 1989. The 5rs of radiobiology. Int. J. Radiat. Biol. 56, 1045–1048. https://doi.org/10.1080/09553008914552491.

Tomagra, Giulia, Aprà, P., Battiato, A., Collà Ruvolo, C., Pasquarelli, A., Marcantoni, A., Carbone, E., Carabelli, V., Olivero, P., Picollo, F., 2019a. Micro graphite-patterned diamond sensors: towards the simultaneous in vitro detection of molecular release and action potentials generation from excitable cells. Carbon N. Y. 152, 424–433. https://doi.org/10.1016/j.carbon.2019.06.035.

Tomagra, Giulia, Franchino, C., Pasquarelli, A., Carbone, E., Olivero, P., Carabelli, V., Picollo, F., 2019b. Simultaneous multisite detection of quantal release from PC12 cells using micro graphitic-diamond multi electrode arrays. Biophys. Chem. 253, 106241 https://doi.org/10.1016/j.bpc.2019.106241.

Tomagra, Giulia, Picollo, F., Battiato, A., Picconi, B., De Marchis, S., Pasquarelli, A., Olivero, P., Marcantoni, A., Calabresi, P., Carbone, E., Carabelli, V., 2019c. Quantal release of dopamine and action potential firing detected in midbrain neurons by multifunctional diamond-based microarrays. Front. Neurosci. 13 https://doi.org/10.3389/fnins.2019.00288.

Uzansaguy, C., Cytermann, C., Brener, R., Richter, V., Shaanan, M., Kalish, R., 1995. Damage threshold for ion-beam-induced graphitization of diamond. Appl. Phys. Lett. 67, 1194–1196. https://doi.org/10.1063/1.115004.

Venton, B.J., Wightman, R.M., 2003. Psychoanalytical electrochemistry: dopamine and behavior. Anal. Chem. 75, 414 A–421 A. https://doi.org/10.1021/ac031421c.

Verona, C., Magrin, G., Solevi, P., Bandorf, M., Marinelli, M., Stock, M., Verona Rinati, G., 2018. Toward the use of single crystal diamond based detector for ion-beam therapy microdosimetry. Radiat. Meas. 110, 25–31. https://doi.org/10.1016/j.radmeas.2018.02.001.

Westerink, R.H.S.S., Ewing, A.G.A., 2007. The PC12 cell as model for neurosecretion. Acta Physiol. 192, 273–285. https://doi.org/10.1111/j.1748-1716.2007.01805.x.

Ziegler, J.F., Ziegler, M.D., Biersack, J.P., 2010. SRIM - the stopping and range of ions in matter (2010). Nucl. Instrum. Methods Phys. Res. Sect. B Beam Interact. Mater. Atoms 268, 1818–1823. https://doi.org/10.1016/j.nimb.2010.02.091.

Zou, M., Bohon, J., Smedley, J., Distel, J., Schmitt, K., Zhu, R.-Y., Zhang, L., Muller, E.M., 2020. Proton radiation effects on carrier transport in diamond radiation detectors. AIP Adv. 10, 025004 https://doi.org/10.1063/1.5130768.